N93-14747

Flow Behavior in Liquid Molding

D. Hunston, F. Phelan, and R. Parnas
National Institute of Standards and Technology
Polymers Division
Gaithersburg, MD

ABSTRACT

The liquid molding (LM) process for manufacturing polymer composites with structural properties has the potential to significantly lower fabrication costs and increase production rates. LM includes both resin transfer molding and structural reaction injection molding. To achieve this potential, however, the underlying science base must be improved to facilitate effective process optimization and implementation of on-line process control. The National Institute of Standards and Technology (NIST) has a major program in LM that includes materials characterization, process simulation models, on-line process monitoring and control, and the fabrication of test specimens. The results of this program are applied to real parts through cooperative projects with industry. The key feature in the effort is a comprehensive and integrated approach to the processing science aspects of LM. This paper briefly outlines the NIST program and uses several examples to illustrate the work.

INTRODUCTION

Polymer based composite materials have much to offer in a wide range of products, particularly in structural applications. Despite the advantages, however, composites have realized only a small fraction of their potential. The most important barrier to their expanded use is the inability to make them rapidly, reliably, and cost effectively. Rejection rates in manufacturing are often too high, and the labor intensive manufacturing methods now used are slow and costly. The solution to this problem is the implementation of more effective processing methods and the development of the scientific understanding necessary to optimize their use.

The process known as liquid molding (LM) has great potential in this regard. LM includes both resin transfer molding (RTM) and structural reaction injection molding (SRIM), which is a high speed cousin to RTM. LM combines some of the speed advantages of simple injection molding with the ability to make the high performance parts associated with continuous fiber reinforcement. Flexibility in the type, amount, and orientation of the reinforcement in every section of the mold enables the generation of very complex parts. Moreover, since the resin viscosity is low, the parts can be quite large and three dimensional.

Because of these potential advantages, LM is the leading candidate for the fabrication of structural composite parts in the automotive industry. Likewise, the drive for more cost effective

manufacturing has caused a variety of other industries including aerospace and marine to consider LM. Effective utilization of this processing method, however, requires developments in both preform fabrication and the technology required for process optimization and on-line process control. Because this technique has such great potential, the National Institute of Standards and Technology (NIST) has initiated a major program to address the scientific issues associated with process optimization and control. This paper will give a general overview of the NIST program and then illustrate the work with two examples from the program.

NIST PROGRAM OVERVIEW

The LM program at NIST has four tasks which are summarized in Table I. Each will be briefly discussed in the material that follows.

Table I:
NIST Program on Liquid Molding

- Materials Characterization
  - Permeability
  - Thermal and Cure Behavior
- Process Simulation
  - Macroscopic Models
  - Microscopic Models
- Process Monitoring / Control
  - Flow Behavior
  - Thermal and Cure Monitoring
- Sample Preparation and Application to Parts

Materials Characterization

The first task focuses on characterization of the material properties associated with processing, i.e. preform permeability, thermal conductivity, and cure behavior. Preform permeability measures the resistance offered by the preform to the flow of a resin. Since the reinforcement can have very different resistances to flow in different directions, the permeability, **K**, is a tensor quantity. This means a variety of measurements both in the plane and through the thickness of the preform material must be conducted to evaluate **K**. The resistance to flow is also very sensitive to the fiber volume fraction so this dependence must be determined. The most direct procedure to measure permeability is unidirectional flow experiments, and a variety of special molds have been developed at NIST to minimize edge effects and facilitate measurements at a variety of fiber volume fractions. For those cases where the part of interest has a shell-like

structure which permits the use of two dimensional flow models, it may be adequate to determine only the in-plane components of the permeability, and this significantly simplifies the characterization.

This task also has the goal of developing the technology to predict the permeability from a knowledge of preform microstructure and fiber surface treatment. This would be a very significant advance because the preform could then be designed to optimize both performance and processibility. Although this technology is well beyond current capabilities, it is an important long range objective. An example of research in this area is given later in this paper.

The measurement of thermal and cure properties for the materials involved relies heavily on the process monitoring facilities established at NIST over the last five years. The objective in developing these facilities was to take advantage of NIST's position as an outstanding measurement laboratory by assembling a wide range of process measurement techniques including virtually all the commonly used methods. Table II lists the ten different techniques that have been adapted to process monitoring in this program. This capability permits the examination of the chemical and physical changes that occur during processing at size scales ranging from individual chemical bonds where the chemistry occurs up to bulk properties such as viscosity and viscoelasticity. By applying these techniques both individually, and in combinations, a detailed picture of the changes can be achieved.

Table II: PROCESS MONITORING TECHNIQUES

Size Scale		
Chemical Bond	Molecules	Bulk
Optical Spectroscopy Calorimetry	Conductance Dielectric Spectroscopy Fluorescence Spectroscopy Chromatography SANS[1]	Ultrasonics Dynamic Mechanical Viscosity
Measurement Methods		

[1]Small Angle Neutron Scattering

Process Simulation

The second task in the NIST program is the development of process simulation models. The models fall into two somewhat arbitrary categories, macroscopic and microscopic. The macroscopic models employ the so called volume averaging approach. This approach focuses on volume elements that are large enough so that variations in local features such as the arrangement of individual fibers in space, interactions between fluid and fibers, etc. average out and thus only the average properties need to be considered. Such treatments are generally quite

good for analyzing macroscopic events such as mold filling.

The macroscopic models are less useful, however, for predicting other important events like void formation since these events depend on local features. To deal with this, microscopic models are needed. Such models include some or all of the local features. In principle, it is possible to simulate the entire part at this level of detail, but the computational time required is prohibitive. As a result, events dependent on local features are simulated by first using macroscopic models of the part to predict boundary conditions on the local area and then simulating this area using a microscopic model.

To analyze complex geometries, the process simulation models are applied using finite element methods. In the NIST research effort, a variety of mold filling programs have been developed (1). The simplest is a 2D program, which is appropriate for flat, thin structures. The most general is a fully 3D program which is used for complex parts with thick sections. Bridging the gap between these is what is called a 2.5D model. This is for flow in shell-like structures in which locally there is always a plane with a thickness dimension that is small compared to the dimensions in the local plane. In these parts, it is assumed that there is no flow in the thickness direction, and thus, the flow is treated as two dimensional even though the structure is three dimensional. Both the 2D and 2.5D programs have significant computational speed advantages relative to the fully three dimensional program, which is the primary advantage of their use. The 2.5D and 3D simulations both account for the effect of gravity on the flow.

Process simulations must analyze many factors including resin flow, heat transfer, chemical reactions, etc., as well as the interactions between these factors. Chemical reactions, for example, generate heat which must be considered in the heat transfer relationships. In certain cases, it is possible to separate some of these factors and thereby simplify the modeling. Often, the mold filling may be completed before the chemical reactions produce significant effects. When possible, the use of such simplifications can significantly accelerate the analysis.

Process Monitoring / Control

The third task in the NIST program involves on-line process monitoring. The purpose is to develop this technology and then use it to address two areas. First, the experiments seek to test and refine the process simulation models. Second, the technology for on-line process control is explored for those situations where it is appropriate. For testing the simulation models, the first step is an examination of flow behavior in mold filling. The principle tool is flow visualization experiments. One drawback of this approach, however, is that visualization which is performed with molds having one or more clear sides provides information only about what is happening at the surface. Consequently, sensors such as fiber optic probes are being developed to measure flow front position inside the preform. Such sensors may also have the potential to measure flow velocity and pressure if properly optimized for LM experiments. The area of cure monitoring is also an important part of the program. Cure monitoring has been a major focus of NIST's research for some time. A detailed examination of the monitoring techniques listed in Table II was conducted to identify those that have the potential for on-line measurement. One result of this effort was a recent report (2) which provides an assessment of the state-of-the-art

process monitoring sensors for polymer composites. The preparation of this report was greatly facilitated by the fact that NIST had direct experience with all of the techniques involved. This capability will now be exploited through application to liquid molding.

Sample Preparation and Application to Parts

The final task involves the fabrication of samples for testing in another NIST program which considers the performance and durability of polymer composites. In addition, this task is applying the developments in the LM program to the study of real parts through cooperative efforts with industry. The best example is a program between NIST and the Automotive Composites Consortium (ACC). The ACC is a joint effort between Ford, Chrysler, and General Motors and was formed to conduct precompetitive research that promotes the use of composites for structural applications in automobiles. The ACC is demonstrating the results of their research by fabricating a series of parts. The first part chosen was the front end structure of the Ford Escort, and the fabrication method of choice was SRIM.

NIST is cooperating with the ACC by conducting process simulations to help optimize the fabrication of this part. In addition, the permeabilities for the reinforcement materials used in the part are being measured at NIST. The ACC benefits by the development of the technology to optimize part design and manufacturing. NIST benefits by having the opportunity to test research results with application to a real part. The initial process simulation focuses on mold filling and uses a 2.5-dimensional model with gravity since the part is a shell-like structure. The complexity of the reinforcement, however, may make it necessary to employ a fully three dimensional flow model eventually. To better visualize the mold filling, a computer animation program has been developed. It allows examination of the mold filling from any angle and permits halting the flow temporarily at any point for closer examination of the details of the filling pattern. Important events such as the closing off of an unfilled area and the formation of knit lines can be seen and studied much more easily with the animation than with the normal output from process simulations.

EXAMPLES FROM THE NIST PROGRAM

To illustrate the NIST program, two examples will be briefly outlined. More details on these particular studies can be found in references 3 and 4. The first example looks at the prediction of permeability and illustrates the use of microscopic flow models and how they can help to examine the effects on flow behavior of localized features such as the distribution of fibers in space. The second example examines two techniques that are commonly used to measure permeability and compares the results. This work illustrates the research in both materials characterization and flow visualization.

Permeability Prediction

Macroscopic models for fluid flow in LM are usually based on Darcy's law

$$\langle \mathbf{v} \rangle = -\frac{\mathbf{K} \cdot \nabla \langle P \rangle}{\mu} \qquad (1)$$

where <v> and <P> are the volume averaged velocity and pressure, respectively, **K** is the permeability of the porous medium, and μ is the viscosity. These models are the basis for most process simulation programs including those developed at NIST (1). One of the most important factors affecting the agreement between the actual filling of a part and the predictions of such process simulation programs is the accuracy of the permeability data available. At the present time, the best and essentially the only method for determining the permeability is through experimental measurements (3,5-7). While this is satisfactory in the sense that various techniques give consistent results (3), and hence, appear to be reliable, it is also desirable to have available theoretical models which can accomplish this. Such models would not only permit optimization of preform structure but also greatly increase the speed with which LM processes could be implemented and/or modified by eliminating (or reducing) the large number of carefully controlled experiments that are currently required for determining the necessary permeabilities.

A number of theoretical models for predicting permeability as a function of structure in fibrous porous media are available (8-10). The most widely used relation in composite applications is the Carman-Kozeny equation which for fibrous porous media is given by

$$K = \frac{\epsilon^3}{(1-\epsilon)^2} \frac{d^2}{16 c_K} \qquad (2)$$

where ϵ is the porosity, d is the diameter of the fibers which make up the media, and c_K is the Kozeny constant which has a theoretical value of 2. While some studies have reported success with this equation (11,12), generally such success is over a limited porosity range with a value of the Kozeny constant much different from its theoretical value (13).* Such limited success is somewhat typical. Therefore, at this time, there is not available a general relation which describes the permeability of fibrous porous media over the entire range of porosities that are of interest.

In order to aid the development of theoretical models for permeability, various numerical studies have been undertaken with microscopic models (14-17*). In such studies, flow in ideal periodic arrays of cylinders (or some other appropriate structure) is modeled, from which predictions for permeability as a function of structure are calculated. Corresponding experiments on systems which closely resemble the idealized arrangements have also been conducted. A review of the relevant experimental and numerical results for fiber porous media has recently been completed (13). An interesting result for the case of axial flow through unidirectionally aligned fiber beds is that experimental measurements (11,18) consistently yield higher permeability values than those predicted by simulation (15). The same result holds true for the case of transverse flow (13). Thus, there is difficulty in matching experimental results not only with theoretical relations such as Carman-Kozeny but also with detailed simulation.

One possible reason for this discrepancy between simulation and experiment is that the materials used in LM preforms are heterogeneous in the sense that the network of fiber bundles

*personal communication,

(tows) which make up the global porous medium are themselves porous. Thus, in actual materials, there is flow not only around but through the tows. The effect of this heterogeneous structure on unsteady flow transients, void formation and ultimate properties has recently been discussed (19,20) and shown to be quite important. Therefore, it seems reasonable to investigate the effect of this property on the permeability as well.

The numerical study of the microscopic flow in fibrous porous media is complicated by the fact that this problem involves both open regions (the space between tows) and porous media (the tows themselves). The flow in the open media can be modeled using the Navier-Stokes equation. The flow in the porous media might be modeled using Darcy's law, but with this approach it is not possible to properly handle the interface between the two regions because the order of Darcy's equation does not allow for the proper specification of boundary conditions (i.e., continuity of velocity and stress) at interfaces. The approach used in this study to achieve the correct degree of continuity is to model the flow in the porous region using the Brinkman (21,22) form of the volume averaged momentum equation (denoted hereafter as BVAME) which is given by

$$\mu\nabla^2\langle \boldsymbol{v}\rangle - \mu\boldsymbol{K}^{-1}\cdot\langle \boldsymbol{v}\rangle = \nabla\langle P\rangle \qquad (3)$$

It is interesting to note that if only the first term on the left were present, the result would be mathematically equivalent to Stokes equation while if only the second term on the left were present, the relationship would be identical to Darcy's law. The most important feature of Brinkman's equations, however, is the presence of second order terms. When this relationship is used to describe the flow in the porous region, the second order terms make it possible to satisfy the boundary conditions at the interface with the open region where Stokes law is used to describe the flow. A variety of problems involving heterogeneous media have been successfully treated using this equation (23,24). While more general expressions than Eq. (3) are available (11,15,25,26) Eq. (3) represents the simplest and most easily applied form.

Simulation

The BVAME was used to develop a microscopic model for flow to elucidate the effect that tow permeability had on the overall permeability in fibrous porous mediums. The axial flow in a periodic, square array of cylinders acting under the influence of a constant pressure gradient of value -G was simulated for the case of both solid and porous cylinders. The computational domain for these geometries is depicted in Figure 1. The problem was scaled using the cylinder diameter, d, as the characteristic length, and a characteristic velocity of d^2G/μ. The relevant component of Eq. (3) is then

$$\frac{\partial^2 U}{\partial X^2} + \frac{\partial^2 U}{\partial Y^2} - \frac{a}{K^*}U = -1 \qquad (4)$$

where X, Y, U, and K^* are the dimensionless coordinates, velocity, and permeability, and a is a computational parameter equal to 1 in porous media, and 0 in open media. Solutions to this set of equations using the appropriate boundary conditions were generated using a Galerkin finite element scheme. Details of the boundary conditions and numerical formulation are discussed in

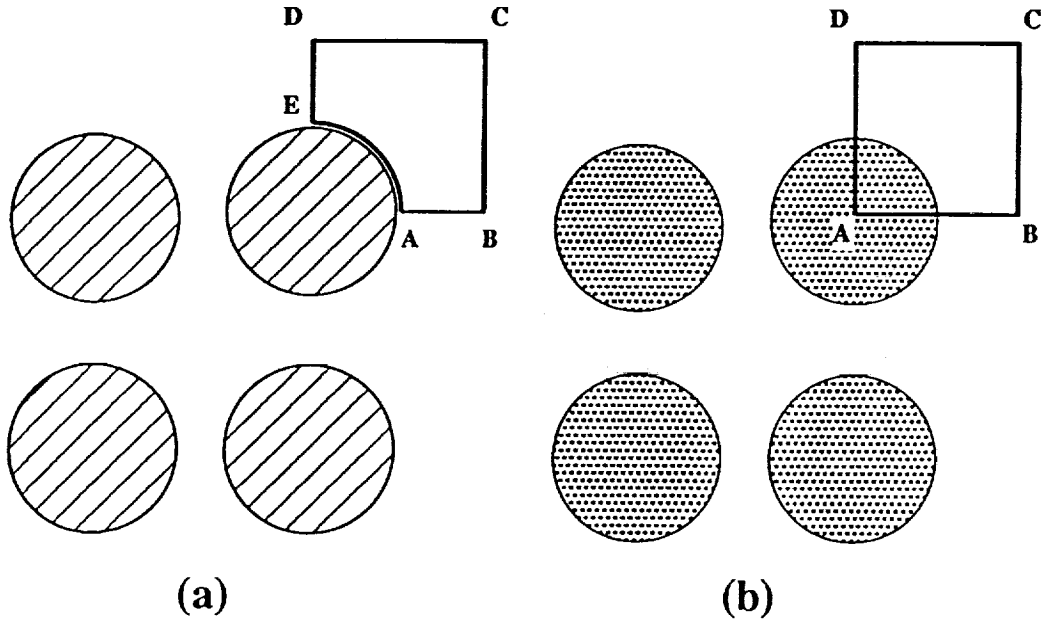

Figure 1: Model for flow simulation for (a) solid and (b) porous cylinders. The unit cell is indicated by the marked area.

detail elsewhere (4).

Calculations were performed for the case of solid cylinders first to verify the numerical scheme by comparing with other calculations, and also, to provide a reference point for looking at porous cylinder results. Figure 2 summarizes the computations by showing the dimensionless effective permeability (i.e., K/d^2) as a function of the porosity. Although not shown in the Figure, the results from the calculations performed here agree quite well with the computations by Sparrow and Loeffler (27). For the sake of comparison, the predictions of the Carman-Kozeny equation and experimental data of Gutowski et al. (11) are also plotted. The Carman-Kozeny results match the numerical calculations only at intermediate to low porosities, and deviate strongly at the extremes. This is similar to what is generally found when comparing Carman-Kozeny to experimental data for systems with solid fillers (13). The most significant observation from the Figure, however, is that the experimentally determined values of dimensionless permeability with porous tows are much higher than any of the numerically calculated and theoretical curves for solid cylinders.

Calculations for porous cylinders were performed with cylinder permeabilities of 0.1, 0.01, 0.001, and 0.0002. Iso-velocity contours (at the same contour values) for solid and permeable cylinders at a cylinder spacing corresponding to an overall porosity of 0.65 are compared in Figure 3 for the case of a cylinder permeability equal to 0.001. The Figure shows that the effect of the cylinder permeability is to shift the contour values inward towards the axis of the cylinder. This shifting results in an increase in the overall flow rate throughout the system.

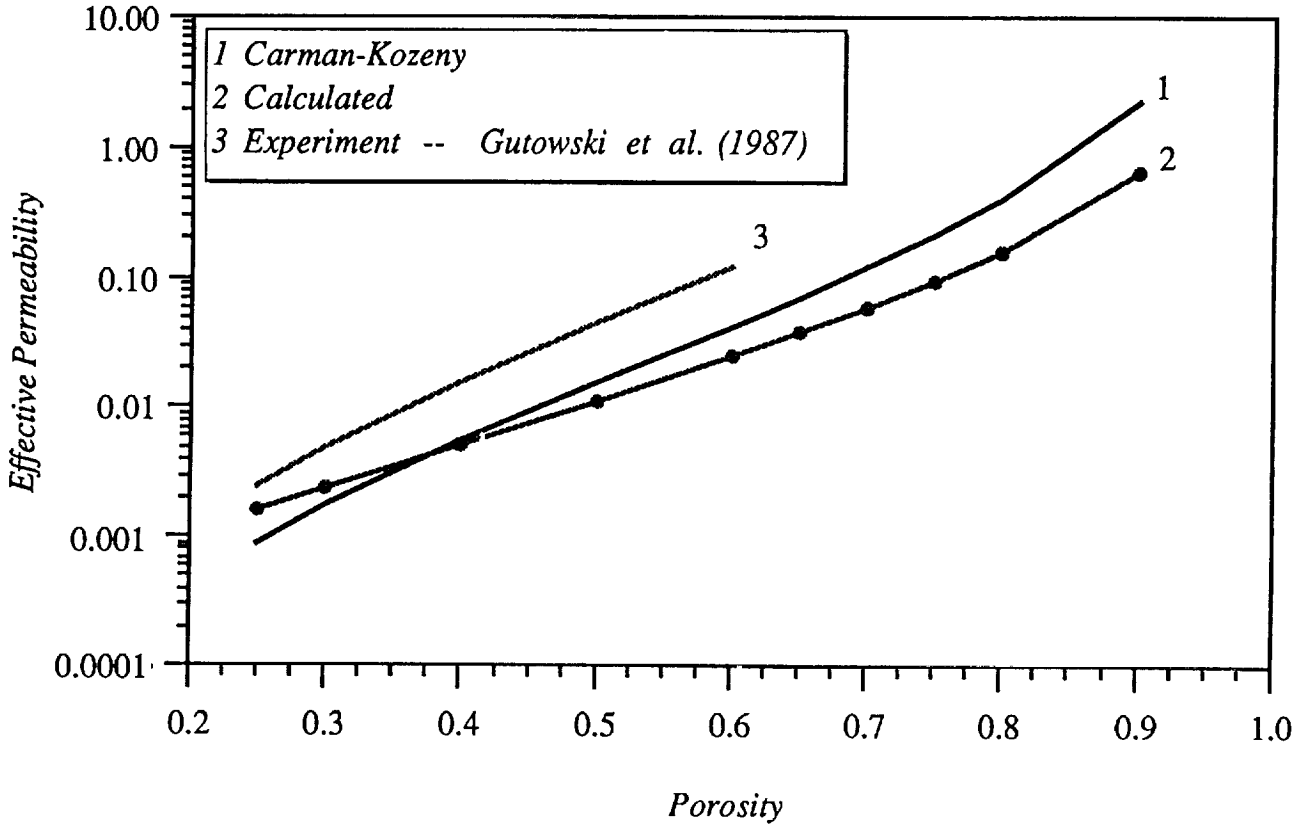

Figure 2: A comparison of the calculated and experimental values for effective permeability as a function of overall porosity.

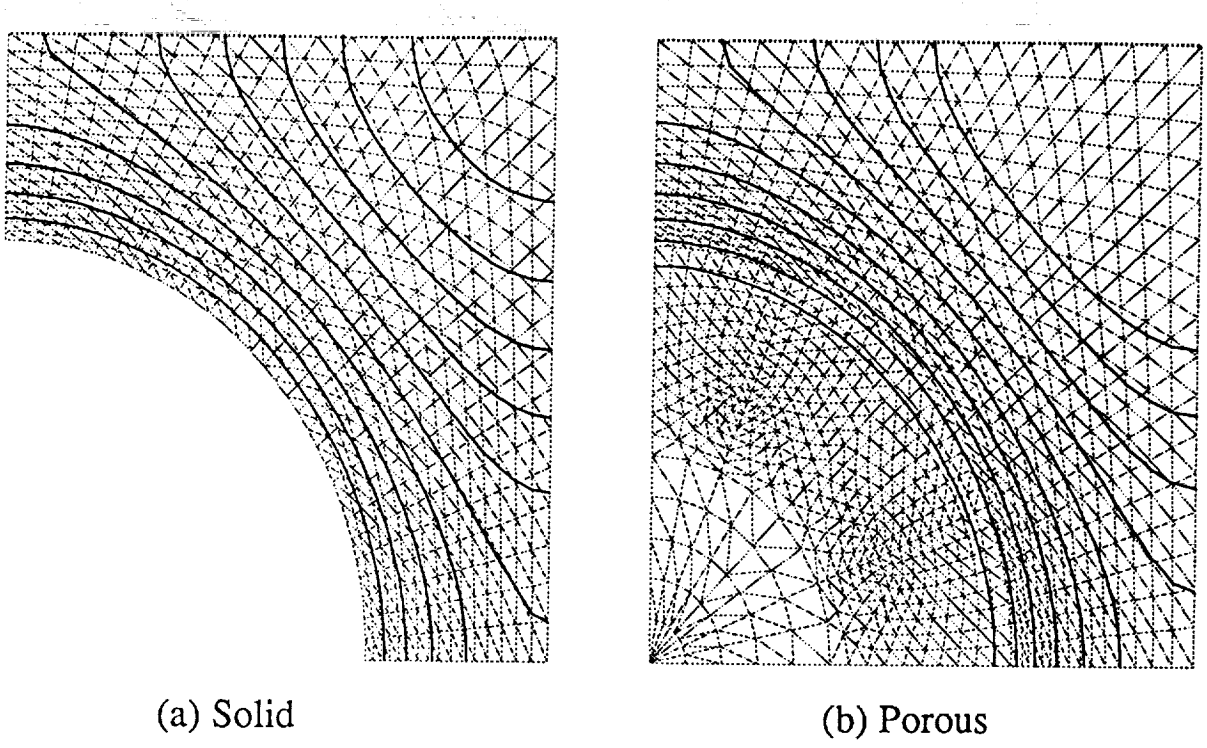

Figure 3: Iso-velocity contours for axial flow through periodic, square arrays of (a) solid and (b) porous cylinders. There are ten equally spaced contours. The maximum velocity for both cases occurs at the upper right-hand corner. The permeability of the porous cylinder is 0.001.

To further quantify this, the ratio of the flow rate in the open media portion of the porous cylinder flow to the flow rate for the solid cylinder flow, as a function of inner cylinder permeability, was computed for cylinder spacings corresponding to porosities of 0.9 and 0.65. This is shown in Figure 4. As was expected from inspection of the velocity contours, the results show that there is a significant flow rate enhancement due to cylinder permeability. The level of enhancement properly converges towards zero as the inner cylinder permeability decreases. Perhaps the most interesting feature of Figure 4 is that it shows that the flow rate enhancement due to the permeability of the cylinder becomes more important as the cylinder volume fraction increases. Thus, even at a cylinder permeability of 0.0002, the flow enhancement is still over 13% (see Table III).

When examining these results, it is important to note that although there is flow through

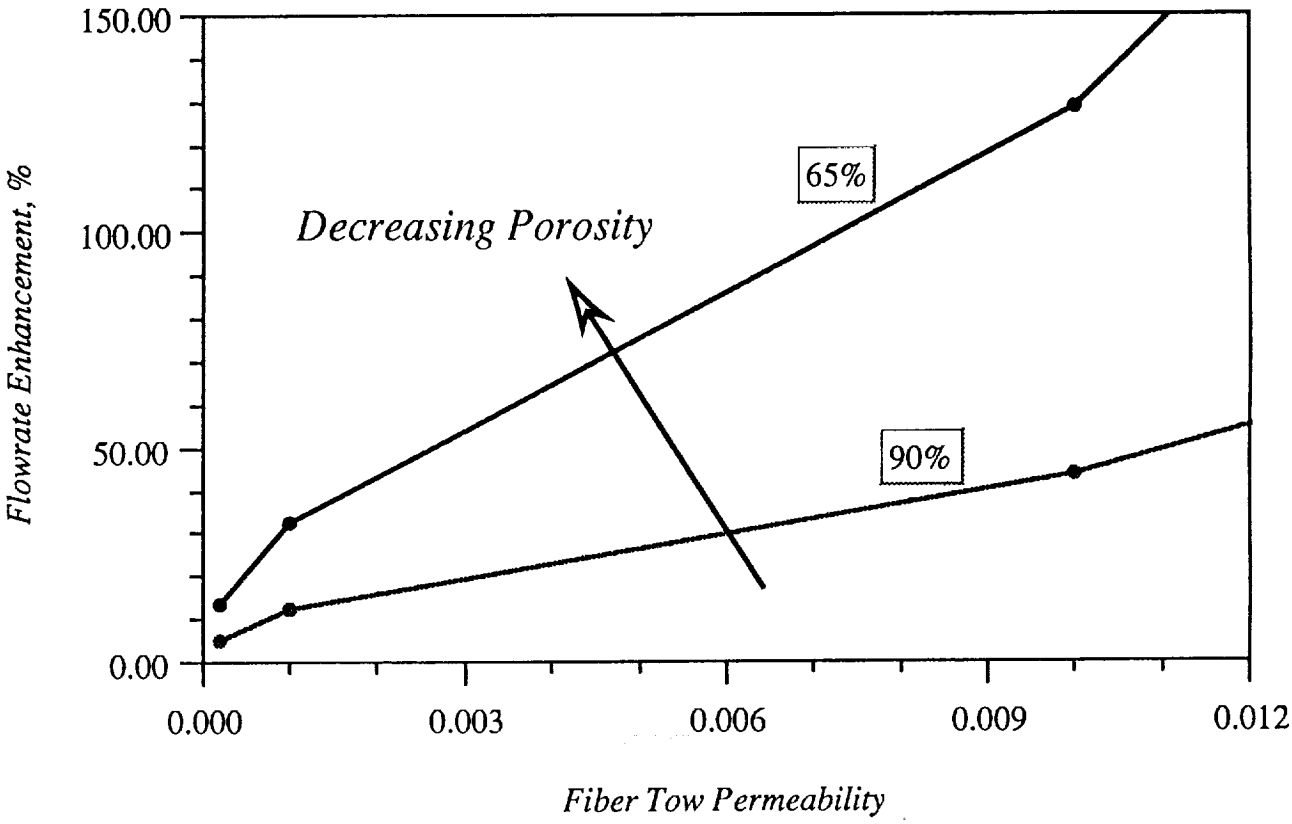

Figure 4: The percentage increase in the flow rate outside the porous cylinder with respect to the case of solid cylinders as a function of tow permeability. The effect becomes more pronounced as the overall porosity decreases.

the porous cylinders, this flow is quite small, and in fact, almost negligible compared to the overall flow rate. The real mechanism for the flow increase is the change in boundary conditions at the cylinder surface which shifts all of the flow contours in Figure 3 toward the center of the porous cylinders relative to the case for solid cylinders. This causes an increase in velocity throughout the entire flow field. Note particularly the increase in the size of the cross-sectional area at the highest flow velocity (upper right corner in Figure 3). Since the flow rate is the integral of the velocity taken over the entire flow domain, the overall change in this quantity is quite substantial.

Table III: Flow Rate Enhancement vs Fiber Tow Permeability

Fiber Tow Permeability	Flow Rate Enhancement (%)	
	Porosity = 0.90	Porosity = 0.65
0.1	225.0	749.6
0.01	43.7	128.8
0.001	12.1	32.7
0.0002	5.1	13.6

Summary

The calculations presented here indicate that the heterogeneous nature of the LM preform material can have a significant effect on the permeability. The calculations predict that the flow rate is substantially higher for porous cylinders than for solid cylinders at equal cylinder spacing and that this increase becomes more pronounced as fiber volume fraction increases. This is consistent with results in the literature where experimentally determined values of permeability in such model networks are generally found to be higher than their theoretical counterparts (13). The results here show that in such situations, the permeability of the tows provides a potential mechanism for flow rate enhancement, and hence, an increased permeability. At this time, calculation of an effective permeability for the overall medium for the case of porous cylinders has not been attempted. This will be done in the future, but requires intra-tow permeability vs. porosity data which is not presently available. Nevertheless, the results obtained here suggest that in order to develop theoretical relationships for permeability as a function of structure in fibrous porous media, it is important to take into account the intra-tow properties of the media.

Permeability Determination

The second example from the NIST program concerns the measurement of permeabilities.

Although all components of the permeability tensor can be important, the discussion here will focus on the in-plane components. There are two techniques commonly used to measure the in-plane permeabilities of preform materials. The first involves unidirectional flow while the second focuses on radial flow. As part of a major effort on permeability characterization, the NIST program is working in cooperation with General Electric's Central Research and Development Laboratory to conduct a detailed comparison of results from the two methods. This tests both the experiments and the flow model used to compare the results. In addition, the data are being examined in terms of the structure of the preform material in an effort to understand the observed behavior. The initial experiments involved measurements on three woven glass reinforcements: J.P. Stevens 8-Harness satin, and Carolina Narrow Fabrics 8-Harness satin and Crowfoot weaves.

Characterization of the in-plane permeability requires the determination of three parameters: the two principle permeabilities, K_{11} and K_{22}, and the principal angle, θ, i.e the angle between the warp direction of the preform material and the direction of the larger of the two principal permeabilities. Moreover, the values obtained for the permeabilities are different for measurements of flow into a dry preform and for flow into a preform completely saturated with the fluid. Although explanations for this difference have been offered (19), experimental measurements for both are still required for a complete characterization.

One-Dimensional Flow Experiments

The one-dimensional flow experiments were conducted in a mold with a 152.5 mm x 152.5 mm (6 in. x 6 in.) sample section where the thickness of the test specimen could be adjusted between 3.175 mm and 12.7 mm (0.125 in. and 0.5 in.) (see Figure 5a). The top of the mold was 12.7 mm (0.5 in.) thick plexiglass to permit observation of the flow front, and the flatness of the plexiglass surface was checked during the experiments to detect and prevent problems due to pressure driven deflection. Fluid was forced through the mold from a pressure-pot, and the flow was measured as it entered the mold with a calibrated rotameter and was also monitored at the mold exit with volumetric measurements. Pressures at the mold inlet were measured by transducers that were mounted at two positions on the back face of the mold located at the lower boundary of the reinforcement sample.

The results from the one-dimensional flow experiments were accumulated by measuring, at preset pressure drops, the flow of corn syrup/water solutions through the woven glass fabric, compressed to 12.7 mm (0.5 in.) thickness and previously saturated with the test fluid. As the pressure drop was increased, the flow rate increased linearly (see Figure 6), as expected, for the Newtonian test fluid. Assuming Darcy's law to be valid, the effective permeability of the preform in the flow direction was obtained from the slope of the flow-pressure curve. The linear relationship of the flow and pressure drop qualitatively indicates that pressure induced bending

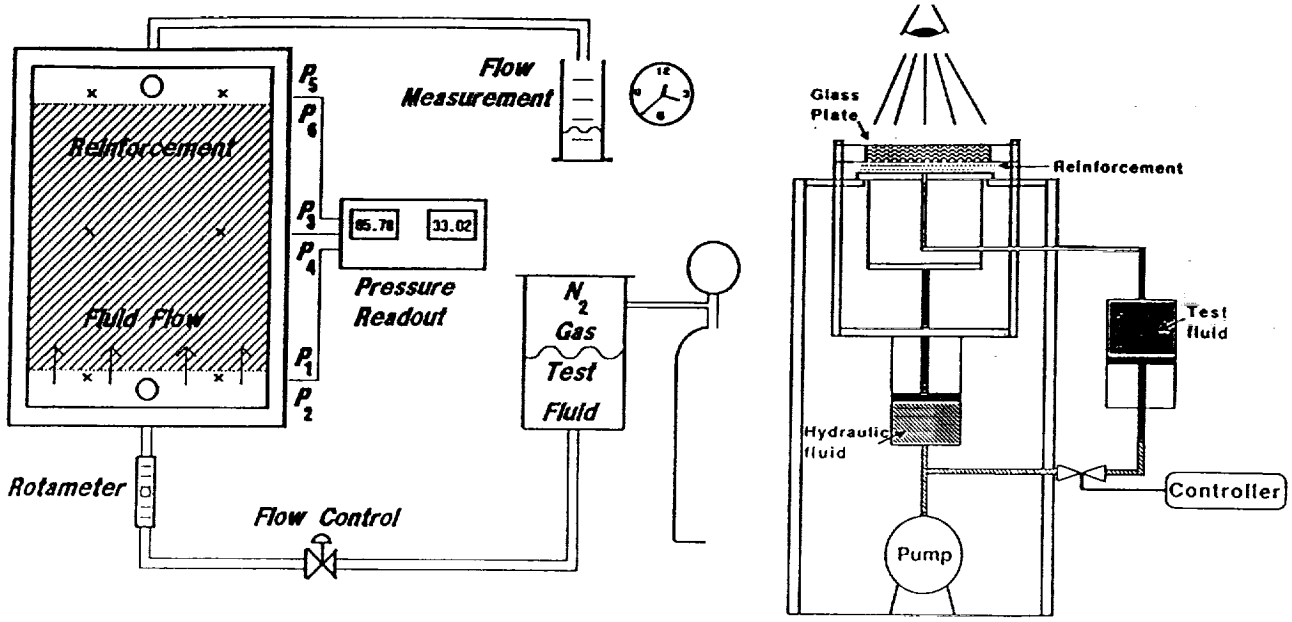

Figure 5: Schematic diagrams of the experimental equipment: (a) one-dimensional flow equipment and (b) radial flow equipment.

of the upper plexiglass plate did not occur. This provides a very accurate way to determine permeability in saturated flow. Since the top of the mold is plexiglass, experiments can also be performed to measure the progression of the flow front into a dry preform. Thus, although the experiments here focused on saturated flow, the permeabilities for both saturated and unsaturated flow can be obtained with this technique.

Radial Flow Experiments

The radial flow experiments were conducted at General Electric's Central Research Laboratory using the apparatus shown in Figure 5b (3). A radial planar flow was achieved by injecting the fluid through a central 1.524 mm (0.060 in.) diameter gate into a 203.2 mm x 203.2 mm (8 in. x 8 in.) region between two parallel plates containing the reinforcement. Each layer of reinforcement had a 4.762 mm (0.1875 in.) diameter hole centered over the gate to permit the fluid to penetrate evenly through the thickness of the sample. A 25.4 mm (1.0 in.) thick upper glass plate permitted visual observation of the flow. A central hydraulic system supplied both the pressure to clamp the reinforcement sample and pump the test fluid from a separate injection cylinder.

After an initial transient, the flow front maintained a shape and orientation that appeared qualitatively unchanged as it grew. Traces of the flow front were made manually, with a typical example shown in Figure 7 for the J.P. Stevens 8-Harness satin weave fabric. Although relatively crude, this presentation technique illustrates important general features of the flow front. The shape of the flow fronts were analyzed by digitizing the traces. For a preform that

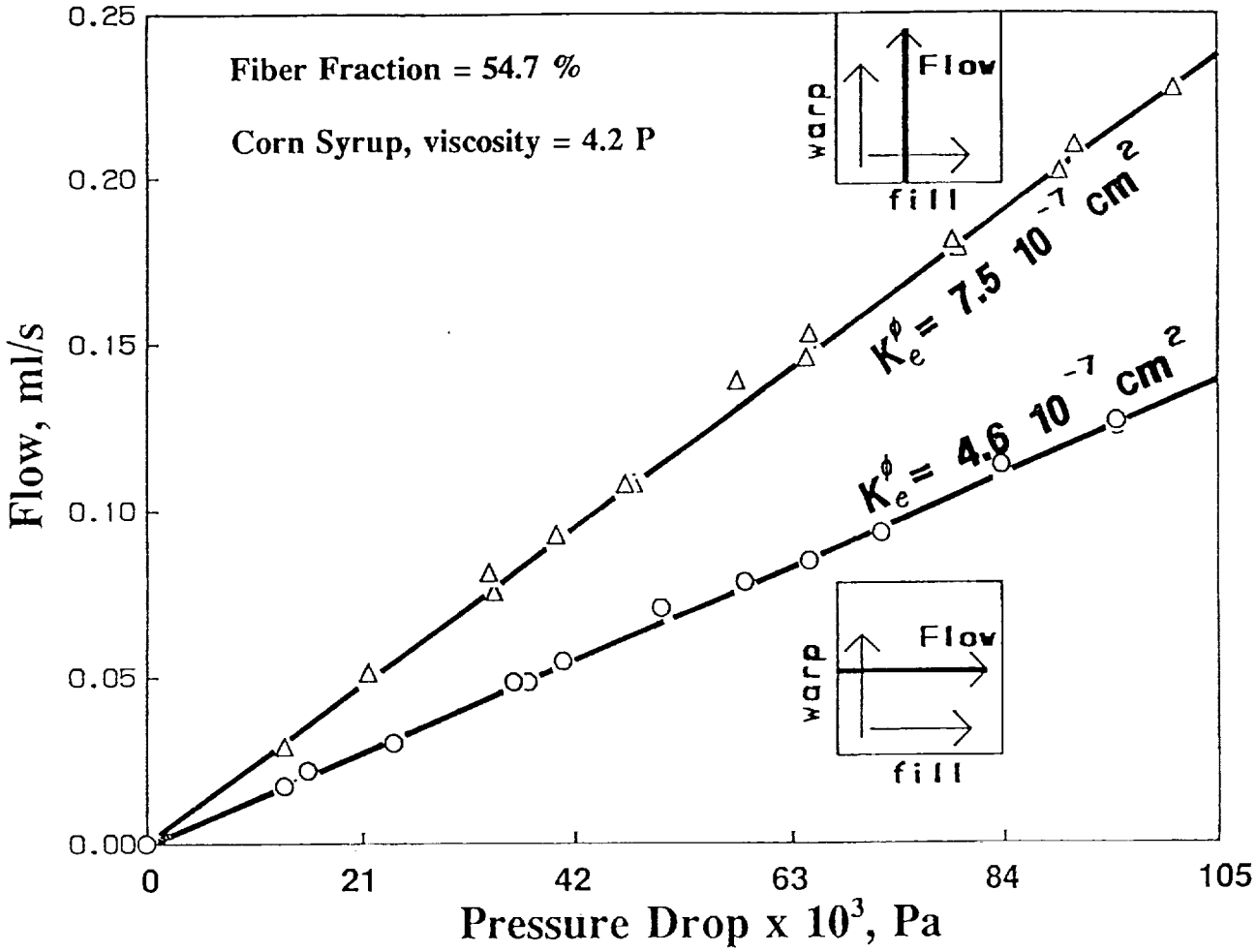

Figure 6: Typical results from a one-dimensional flow experiment showing flow vs. pressure drop for two fabric orientations.

is isotropic in the plane, a circular pattern would be expected. If the permeability in the plane is anisotropic but orthotopic, an elliptical shape should fit the data. For the materials examined here, the flow front was indeed elliptical in shape, and this confirms orthotopic behavior for the high volume fractions tested. The direction of the principal axis of the ellipse relative to the warp fibers in the preform provides a measure of the principal angle, while the square of the ratio of the major to minor axis lengths in the ellipse is equal to the anisotropy which is the ratio of the two principal permeabilities, K_{22}/K_{11}.

As can be seen, the determination of the principal angle and the anisotropy in the radial flow experiment is quite easy. Although it is also possible to determine the quantitative values of the permeabilities, this is more difficult. Moreover, the experiments described above measured

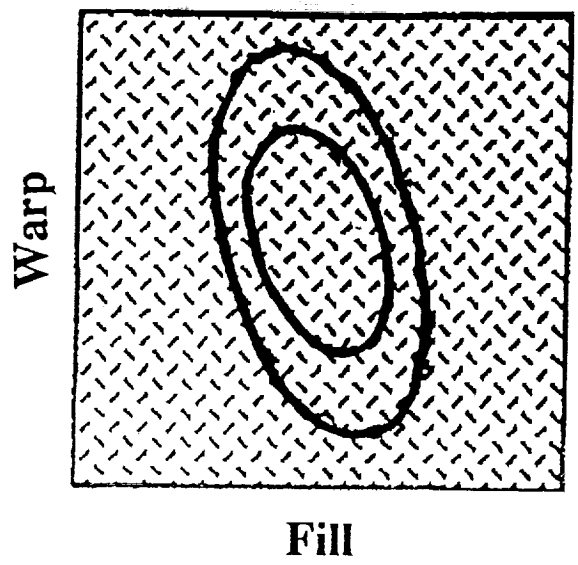

Figure 7: The elliptical flow fronts observed in J.P. Stevens 8-Harness satin fabric.

unsaturated flow properties. Although permeability measurements for saturated flow are possible in the radial flow experiments, they are considerably more difficult. Consequently, the work here focused only on the determination of the principal angle and anisotropy for unsaturated flows and compared the results with values for these parameters obtained from saturated, unidirectional flow experiments.

Comparison of Results

To compare the one-dimensional flow results with the radial flow results, it was necessary to calculate the principal permeabilities and the principal angle from the unidirectional flow experiments. By using a two-dimensional version of Darcy's Law, the effective permeability, K_e^{ϕ}, in a direction which is at an angle, ϕ, relative to the warp direction in the preform can be written in terms of the principal permeabilities and the principal angle.

$$K_e^{\phi} = K_{11}\cos^2(\phi-\theta)\bullet$$

$$\left[\left(1+\frac{K_{22}}{K_{11}}\tan^2(\phi-\theta)\right) - \frac{(K_{22}/K_{11}-1)^2}{\frac{K_{22}/K_{11}}{\tan^2(\phi-\theta)}+1}\right] \qquad (5)$$

Since this equation involves three unknowns, measurements at a minimum of three different orientations must be made. To improve reliability, four orientations were tested in this work. The results of measurements conducted at two orientations are shown in Figure 6. That figure indicates that the permeability is anisotropic which agrees with the radial flow experiments. From the four experiments on each material, the values for the principal permeabilities and the principal angles were calculated for the three materials tested. The results are given in Table IV along with the data obtained in the radial flow experiments. Additional details of the analysis are given in reference 3.

The consistency of the radial flow experiments performed at GE and the one-dimensional flow experiments conducted at NIST is illustrated in Table IV. Even though two different laboratories conducted the experiments, the agreement is quite good. As the experimental techniques are further refined, it will be important to see if the agreement gets even better.

Table IV: Comparison of 1-D and Radial Flow Experiments

Material	Laboratory	Principle Angle	K_{22}/K_{11}
J.P. Stevens 8-H satin	GE	12	0.64
	NIST	13	0.72
Carolina Narrow Fabric 8-H satin	GE	-17	0.77
	NIST	-15	0.73
Carolina Narrow Fabric Crowfoot	GE	3	0.69
	NIST	4	0.61

It is interesting to note that the principal direction of the permeability is not coincident with either the warp or fill yarn directions. An hypothesis for this behavior has been developed based upon a closer examination of the structure of the woven fabrics. The crossing of the fiber tows creates a series of valleys in a woven material known as the crimp. Figure 8 illustrates this structure for the J.P. Stevens 8-Harness satin fabric, and the Carolina Narrow 8-Harness and Crowfoot fabrics used in the experiments reported above. The close proximity of neighboring crossing points creates a nearly continuous trough that may act as a conduit of low resistance to flow.

Note that the orientation of the illustrated crimps in Figure 8 match the orientation of the principal axes of permeability observed in both the radial and one-dimensional flow experiments with the two 8-Harness satin weave fabrics. A secondary, nonorthogonal crimp direction does not appear to influence the flow because the tow crossing points are not on adjacent tows. However, a crimp direction in the Crowfoot weave could not be identified for comparison with the principal axis of permeability in that material. An additional unresolved point in this discussion is that the major crimp directions on opposite sides of the fabrics are not oriented identically, creating a complex interface between fabric layers which must be explored further.

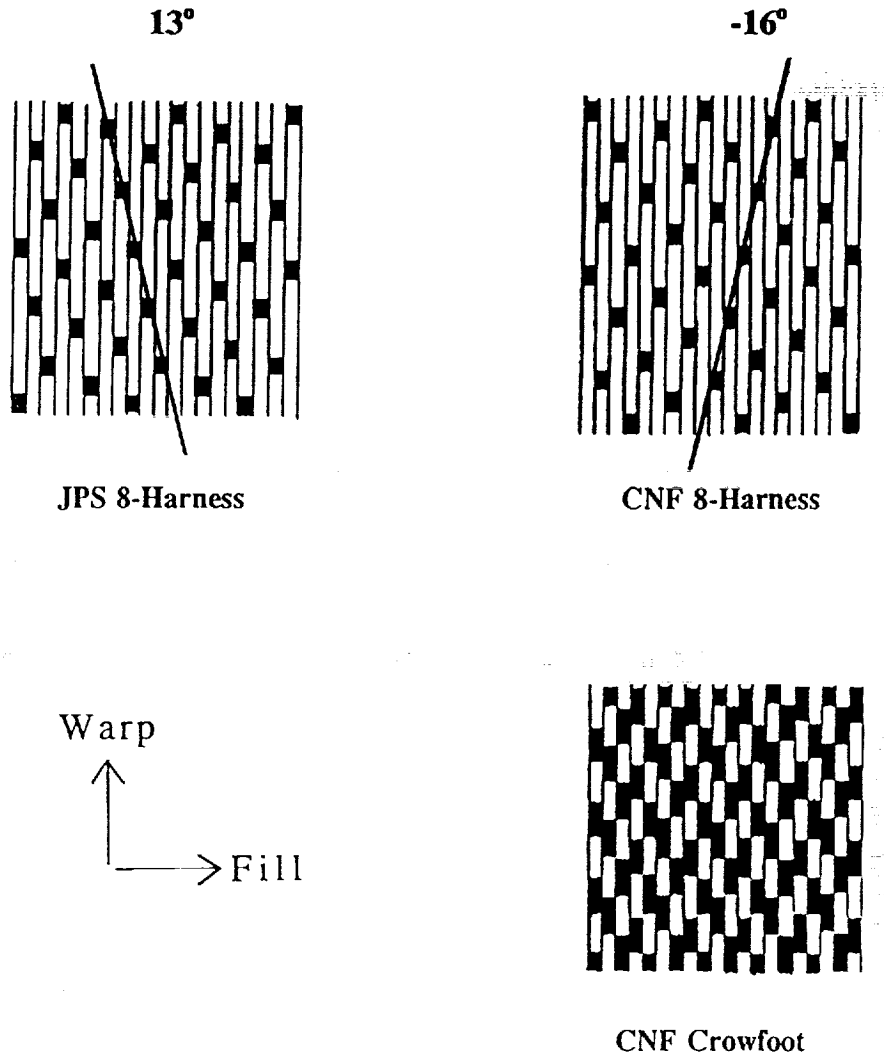

Figure 8: Structure of woven fabrics showing crimp directions. The angle between the crimp direction and the warp fiber direction is indicated. Note that a crimp direction is not apparent in the Crowfoot weave.

The data developed in this project represent a first step in exploring not only the test methods for permeability measurement but also the models used to analyze the data. Constitutive models, such as Darcy's Law, have largely been used without detailed verification. The limited results obtained so far not only indicate that the unidirectional flow and radial flow experiments are consistent but also support the use of Darcy's Law in flow simulations. Since the radial flow experiments quickly provide a measure of flow anisotropy and principal orientation while the one-dimensional flow experiments easily yield quantitative measurements of the permeability, the results also suggest that the two experiments could be used in combination to simplify the characterization of preform materials.

CONCLUSIONS

The program described here seeks to advance the scientific basis for liquid molding through a coordinated effort involving four tasks: (1) characterization of the material properties associated with processing, (2) development of process simulation models at both the macroscopic and microscopic levels, (3) application of on-line measurement techniques to test and refine the simulation models and to explore the technology for on-line process control, and (4) production of test samples and the application of the technology developed in the program to real parts through cooperative interactions with industry. Such a comprehensive and interdisciplinary approach offers the best hope for achieving the full potential of the liquid molding process.

REFERENCES

1. F. R. Phelan Jr., "Liquid Molding: Computer Simulation," p. 36 in "Polymers, Technical Activities 1991," NISTIR-4696, February 13, 1992.

2. D. Hunston, W. McDonough, B. Fanconi, F. Mopsik, F. Wang, F. Phelan, and M. Chiang, "Assessment of the State-of-the-Art for Process Monitoring Sensors for Polymer Composites," U.S. Department of Commerce, NISTIR-4514, June 1, 1991.

3. A. J. Salem, and R. S. Parnas, "Presented at the ASC 6th Technical Conference on Composites," (1991).

4. F. R. Phelan Jr., "Advanced Composite Materials: New Developments and Applications, Proceedings of the 7th Annual ASM/ESD Advanced Composites Conference," 175, ASM International, (May 1991).

5. K. L. Adams, and L. Rebenfeld, Textile Research Journal, 57, 647-654, (November 1987).

6. K. L. Adams, B. Miller, and L. Rebenfeld, Polymer Engineering and Science, 26(20), 1434-1441, (November 1986).

7. C. A. Fracchia, "Numerical Simulation of Resin Transfer Mold Filling," M.S. Thesis, University of Illinois at Urbana-Champaign, (January 1990).

8. R. Gauvin, and M. Chibani, SAMPE Quarterly, 21(5), 52-58, (1990).

9. R. K. Young, S. P. McCarthy, J. P. Fanucci, S. C. Nolet, and C. Koppernaes, SAMPE Quarterly, 22(3), 16-22, (April 1991).

10. R. M. Koerner, J. A. Bove, and J. P. Martin, Geotextiles and Geomembranes, 1, 57-73, (1984).

11. T. G. Gutowski, T. Morigaki, and Z. Cai, Composite Materials, 21, 172-188, (1987).

12. R. C. Lam, and J. L. Kardos, "Proceedings of the Society of Plastics Engineers 48th Annual Technical Conference (Antec '89)," 1408-1412, (May 1989).

13. L. Skartis, J. L. Kardos, and B. Khomani, Materials Research Laboratory and Department of Chemical Engineering, Washington University, St. Louis, MO, 1991.

14. A. S. Sangani, and A. Acrivos, Int. J. Multiphase Flow, 8, 193-206, (1982).

15. R. E. Larson, and J. J. L. Higdon, J. Fluid Mech., 166, 449-472, (1986).

16. R. E. Larson, and J. J. L. Higdon, J. Fluid Mech., 178, 119-1362, (1987).

17. L. Skartis, J. L. Kardos, and B. Khomani, Materials Research Laboratory and Department of Chemical Engineering, Washington University, St. Louis, MO, 1991b.

18. R. R. Sullivan, J. App. Phys., 13, 725, (1942).

19. R. S. Parnas, and F. R. Phelan Jr., SAMPE Quarterly, 22(2), 53-60, (1991).

20. N. Patel, and L. J. Lee, "Proceedings of the Society of Plastics Engineers 49th Annual Technical Conference (Antec '91)," 1985-1990, (May 1991).

21. J. C. Slattery, "Momentum, Energy and Mass Transfer in Continua," Robert E. Kreiger Publishing Company, Huntington, New York, 2nd Edition, Huntington, New York, (1981).

22. H. C. Brinkman, App. Sci. Res., A1, 27, (1947).

23. M. N. Kaddioui, and D. Sigli, Applied Scientific Research, 47, 23-44, (1990).

24. R. Parnas, and Y. Cohen, Chem. Eng. Comm., 53, 3-22, (1987).

25. P. G. Saffman, Stud. Appl. Maths., 50, 93-101, (1971).

26. J. Koplick, H. Levine and A. Zee, Phys. Fluids, 26(10), 2864-2870, (1983).

27. E. M. Sparrow, and A. L. Loeffler Jr., AIChE Journal, 5(3), 325, (1959).